

### Violation of Bell's Inequality over 4 km of Optical Fiber

P. R. Tapster, J. G. Rarity, and P. C. M. Owens

*DRA Malvern, St. Andrews Road, Malvern, Worcester WR14 3PS, United Kingdom*  
(Received 7 March 1994)

Using energy correlated photon pairs created in parametric down-conversion we demonstrate two-photon interference effects in fiber interferometers separated by 4.3 km of optical fiber. The measured 86% interference visibilities confirm the purely quantum mechanical origin of these correlations.

PACS numbers: 42.50.Wm, 03.65.Bz, 42.25.Hz

Energy and momentum correlations are inherent in the creation of two photons from one pump photon in the process of parametric down-conversion [1]. These correlations can be used to produce photon pairs in simple entangled states of the form

$$\Psi = |1\rangle_a|1\rangle_b + e^{i\Phi}|1\rangle_c|1\rangle_d, \tag{1}$$

where  $a, b$  and  $c, d$  are indistinguishable routes from the two-photon source to the detectors and  $\Phi$  is the cumulative phase difference between these two routes. Such entanglement leads to nonlocal interference effects which violate the well-known Bell's [2] inequality. Although initial experiments were confined to spin or polarization correlated photon pairs [3], recent experiments have shown nonlocal interference based on indistinguishability of momenta [4,5] and emission times [6,7]. All of these experiments have been confined to typical length scales less than a few meters between correlated photons. It is of interest to check that these correlations extend to larger distances not only as further confirmation of this counterintuitive property of quantum mechanics but also to confirm the practicality of recent key sharing [8] and "quantum teleportation" schemes [9].

The scheme well suited for extension to large separations is that first suggested by Franson [6] (Fig. 1). Here we create a superposition state of emission times when we cannot distinguish between events where both photons of the pair pass through the long arm of the interferometers and events where both photons pass through the short arms of the interferometers. These events remain coherent with each other when the pump beam coherence length (time uncertainty) is longer than the path difference because of energy conservation in the process of down-conversion. Initial large separation experiments have only shown weak correlations [10–12] because of noninterfering events arising from distinguishable paths in the bulk interferometers used and from events where pairs take different length routes through the interferometers. Here we demonstrate high visibility two-photon interference correlations out to separations of 4.3 km using single mode fibers and low jitter coincidence detection.

We consider the apparatus shown in Fig. 1 where signal and idler arms of the apparatus contain single-mode-fiber Mach-Zehnder interferometers with similar large path length differences  $X_s, X_i$  and phase plates introducing

small phase shifts  $\phi_s, \phi_i$ . The interference effects appear in the rate of coincidence detections between signal  $s$  and idler arms  $i$  of the apparatus. Noninterfering events where one photon takes the short path and the other long path can be discriminated by accurate time-of-arrival measurements when detector resolution  $\delta t < X_{s,i}/c$  [13]. The coincidences can then be resolved into two noninterfering satellite peaks around a central interference peak. Here we select only the central peak and study events where the wave function viewed from the detectors can be simply represented by

$$\Psi_{si}(t, t') = \frac{1}{\sqrt{2}} \int d\omega_s d\omega_i e^{-i(\omega_s t + \omega_i t')} f_s(\omega_s) f_i(\omega_i) \times (|1_{lo}\rangle_i |1_{lo}\rangle_s e^{i(\phi_s + \phi_i)} e^{i[X_s k(\omega_s) + X_i k(\omega_i)]} + |1_{sh}\rangle_i |1_{sh}\rangle_s), \tag{2}$$

where we assume 50/50 beam splitters,  $|1\rangle_{s,i}$  denotes a one-photon state in the signal or idler arm of the apparatus and the subscripts lo and sh denote propagation via the long and short paths through the interferometer.  $\omega_s$  and  $\omega_i$  are angular frequencies of the down-converted photons and we integrate over normalized filter functions  $f_{s,i}(\omega_{s,i})$ .

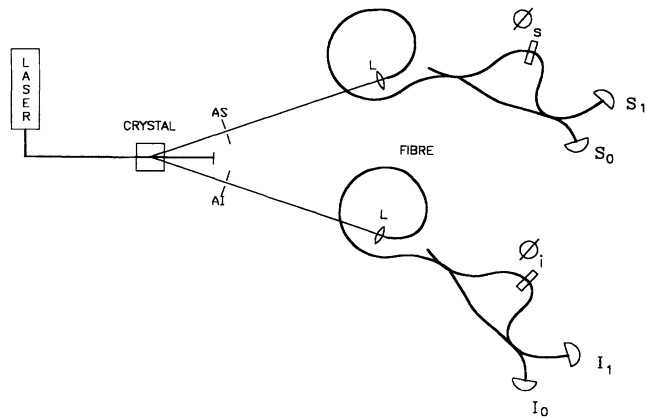


FIG. 1. Franson's experiment adapted to parametric down-conversion and fibers. A pump laser illuminates a suitably cut nonlinear crystal. Pair photons are selected by apertures (AS,AI) and launched by lenses  $L$  into optical fibers. Signal and idler photons pass through unbalanced Mach-Zehnder interferometers incorporating phase shifters  $\phi_s, \phi_i$ . Photon-counting detectors  $S_0, S_1$  and  $I_0, I_1$  are connected to the interferometer outputs.

Energy conservation at the crystal confines  $\omega_s + \omega_i = \omega_0$ , where  $\omega_0$  is the pump frequency. This allows use of a single filter function  $f(\omega)$  around center frequencies  $\omega_{sc,ic}$ . We also introduce the wave numbers  $k(\omega_{s,i})$  in the interferometers noting that material dispersion can be included by Taylor expansion

$$k(\omega_s + \omega) = k_s + \alpha_s \omega + \beta_s \omega^2 + O(\omega^3), \quad (3)$$

with  $k_s$  the wave number in the medium at the signal center frequency  $\omega_{sc}$ . For the idler wave number, subscripts  $s$  are replaced by  $i$  and  $\omega$  by  $-\omega$ . Interference effects are retained for large  $X_{s,i}$  as a result of energy conservation, and when the spread of the pump frequency  $\Delta\omega_0$  sets a coherence length longer than the path length difference  $1/\Delta\omega_0 \gg \Delta X/c$ .

The probability  $P_{si}$  of seeing a photon in the signal detector indexed  $p$  (Fig. 1) coincident (within the detector resolution time) with an idler detection in  $q$  is given by [14]

$$P_{si}(p, q) = \frac{1}{2} \eta_s \eta_i [1 + (-1)^{p+q} V \cos(\phi_i + \phi_s + k_s X_s + k_i X_i + \phi_d)], \quad (4)$$

showing a cosinusoidal oscillation dependent on the phase sum  $\phi_i + \phi_s$  (constant phase shift  $\phi_d$  arises from dispersion) and with visibility function  $V \leq 1$  dependent on path length matching and dispersion. The correlation coefficient can be defined as

$$E(\phi_s + \phi_i) = P_{si}(0, 0) + P_{si}(1, 1) - P_{si}(1, 0) - P_{si}(0, 1) / \sum_{p,q} P_{si}(p, q) = V \cos(\phi_s + \phi_i). \quad (5)$$

It has been shown [15] that a measurement of this function showing a visibility above 71% discriminates this as a purely quantum mechanical correlation and rules out all semiclassical and local realistic descriptions of the effects. The apparent nonlocality arises because we can fully redistribute the coincident photodetections at remote locations (from  $S_0I_0$  to  $S_0I_1$ , for instance) by adjusting either of the local phases. As we have no *a priori* knowledge of which output any given photon will appear in (we see no single beam interference) there can be no information sent by this technique. This does not rule out the sharing of random data at the two locations when the phases are adjusted for 100% correlation [8].

Including mismatched interferometers and real dispersion the visibility function  $V$  is given by [16]

$$V = \left| \frac{1}{\sqrt{1 - iD}} \exp \left[ -\frac{\sigma^2(\alpha_s X_s - \alpha_i X_i)}{4(1 - iD)} \right] \right|, \quad (6)$$

with  $D = \sigma^2(\beta_s X_s + \beta_i X_i)$  assuming a Gaussian function of  $1/e$  width  $\sigma$  is used to describe the pair-photon bandwidth. Interferometers are matched when the second

term in the above is made unity by adjusting  $X_s$  or  $X_i$  to equalize pulse propagation times through the extra length. The first term arises from group velocity dispersion (GVD) and can lead to loss of interference visibility when bandwidth  $\sigma$  is large. Group velocity dispersion is quoted as  $dv_g^{-1}/d\lambda = 120$  ps/nm km for 820 nm fiber while at the typical communications wavelengths of  $1.3 \mu\text{m}$  it drops to 3.5 ps/nm km. When we identify  $\beta$  with the quoted values of GVD via

$$\beta = \frac{d^2 k}{d\omega^2} = \frac{\lambda^2}{2\pi c} \frac{dv_g^{-1}}{d\lambda}. \quad (7)$$

We can estimate  $D = 10^{-3} G_{vd} \Delta\lambda^2 \Delta X$ , where  $\Delta\lambda$  is a full width at half maximum (FWHM) filter width (in nm),  $\Delta X$  is measured in meters, and  $G_{vd}$  is the quoted value of GVD in units as above. For  $\Delta X = 0.3$  m and  $\Delta\lambda = 10$  nm we find a  $V > 0.994$  at  $1.3 \mu\text{m}$  but a drastic loss of visibility when working at 820 nm. All factors seem to favor working in the low loss communication band but single photon detector performance at these wavelengths is poor. Here we come to a compromise and use photon pairs centered on  $1.3 \mu\text{m}$  and 820 nm avoiding dispersion effects at the shorter wavelength using an air gap path length difference.

An outline of the experimental apparatus is shown in Fig. 2. Light from a single frequency argon ion laser operating at 501.7 nm is weakly focused into a crystal (CR) of lithium iodate 2 cm long. The crystal is cut and tilted to produce nondegenerate photon pairs of wavelength 820 nm and  $1.3 \mu\text{m}$  propagating at  $4.5^\circ$  and  $7.2^\circ$  to the pump beam. Apertures (AS, AI) are used to select the beams. Further selection is performed by filters FS (an RG850 bandpass filter) and FI (center wavelength 831.6 nm, 9.5 nm FWHM, tilted  $19.3^\circ$  to a center wavelength of 820 nm). Microscope objectives (MS, MI,  $\times 10$ , 0.23 NA) are used to launch the light into single-mode optical fibers.

The 820 nm light passes directly to a 820 nm single-mode fiber interferometer made from two 50/50 fiber couplers. Both arms of this interferometer contain equal

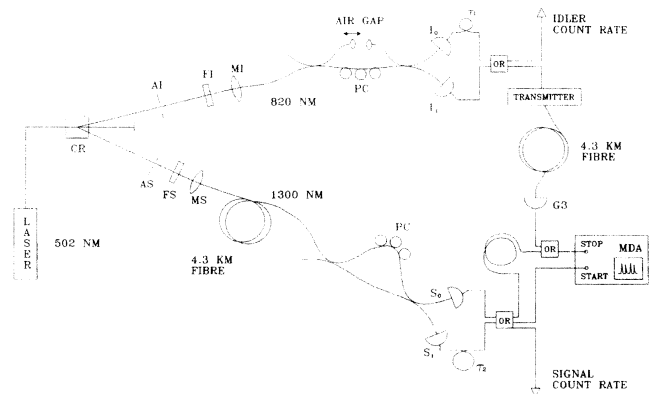


FIG. 2. The experimental apparatus; see text for detailed description.

lengths of glass (to within about 1 mm). The extra path length in the long arm is provided by a 50 cm air gap formed using two fiber launchers and AR-coated ball lenses. This arrangement ensures no loss of visibility due to dispersion as discussed above. One of the launchers is mounted on a computer-controlled motorized translation stage with 0.1  $\mu\text{m}$  resolution and a 5 cm range. Coarse scanning of the translation stage enables us to match the path difference in this interferometer to that in the 1.3  $\mu\text{m}$  interferometer. Fine scanning in 0.1  $\mu\text{m}$  steps is used to observe the coincidence fringes. One arm of the interferometer contains a "bat ear" style polarization controller (PC) consisting of three double loops of fiber, each independently oriented to match polarization states at the second coupler. The outputs of the interferometer are fusion spliced to the two idler detectors  $I_0$  and  $I_1$  silicon avalanche photodiodes with multimode fiber pigtailed (EG&G 30902SQC). For the photon-counting operation, the detectors are biased 30 V beyond breakdown (around  $-250$  V), passively quenched [17] with a 560 k $\Omega$  resistor, and cooled to  $-5^\circ\text{C}$ . With these operating conditions we estimate a detection time jitter of around 600 ps (FWHM).

The 1.3  $\mu\text{m}$  light passes through a 4.3 km reel of single-mode communications fiber before reaching a 1.3  $\mu\text{m}$  fiber interferometer constructed again from two 50/50 fiber couplers fusion spliced together. The path difference between long and short arms was set to the equivalent of 50 cm in air (34 cm in glass or 1.7 ns time difference). A polarization controller consisting of three triple loops of fiber is present in the long arm of the interferometer. The outputs of this interferometer are connected to detectors  $S_0$  and  $S_1$ , germanium avalanche photodiodes (APDs) with multimode fiber pigtailed (NEC type NDL5103P) operating in photon-counting mode [18]. The germanium APDs are biased 0.3 V beyond breakdown (around  $-25$  V), passively quenched with a 33 k $\Omega$  resistor, and operated at 77 K in order to keep the dark counts low. A high speed amplifier increases the pulse heights by a factor of 200 before discrimination. The resulting detection time jitter is around 460 ps FWHM. Pulses from all four detectors are standardized using a high speed discriminator.

The path length differences are matched by connecting the two interferometers in series and illuminating with a 1.3  $\mu\text{m}$  LED behind a 10 nm bandwidth 1.3  $\mu\text{m}$  interference filter. The singles count rate of a germanium detector is monitored as a function of air gap length. Interference fringes are observed in the singles rate when the two path length differences are equal. The 1.3  $\mu\text{m}$  fiber polarization controllers are adjusted to maximize visibility of the second order fringes. The interference filter is finally removed in order to pinpoint the fringe visibility maximum accurately before reverting to the normal operating arrangement depicted in Fig. 2.

In order to measure the correlation coefficient as a function of phase [Eq. (5)] we use the four coincidence rates ( $S_0I_0, S_1I_1, S_0I_1, S_1I_0$ ) from all possible detector combina-

tions. We do this using a *single* time-interval analyzer and the arrangement of time delays and OR gates illustrated in Fig. 2. The outputs from the two silicon detectors are combined in an OR gate, as are the pulses from the germanium detectors. Electronic delays  $\tau_1 = 7.1$  ns and  $\tau_2 = 16.9$  ns then ensure that coincidences from different combinations of signal and idler detectors can be discriminated by delay time (see Fig. 3). For efficient operation of the time-interval analyzer we require a short delay between start and stop pulses and prefer the lower count rate to be the start pulse. For this reason we use the combined signal (germanium) detectors' counts as start pulses. The combined idler pulses are delayed in a classical optical channel consisting of a 1.3  $\mu\text{m}$  transmitter, 4.3 km of communications fiber, and a detector (G3) made of a germanium APD (Fujitsu FPD13R51KS) operating in analog mode at room temperature ( $-30$  V bias, 60 ps jitter in transmitter and receiver). Coincident detections are measured using a Hewlett-Packard HP53110A time-interval analyzer [or modulation domain analyzer (MDA)] capable of collecting time interval histograms at 2.5 MHz. If we had used the silicon detectors as start pulses without the optical delay, the system would have had a 25  $\mu\text{s}$  dead time. Typical count rates for each silicon detector ( $I_0$  and  $I_1$ ) are 90 kHz light and 10 kHz dark (80 kHz net light) and 23 kHz light, 15 kHz dark for each germanium detector ( $S_0$  and  $S_1$ ). Total coincidence rates (in a 30 ns gate) of up to 1.5 kHz were achieved, a typical value being 1 kHz.

A typical time delay spectrum appears in Fig. 3 showing twelve different coincidence peaks grouped in four sets of three. Each set of three represents one of the four possible combinations of signal and idler detectors as labeled. In all cases the satellite peaks arise from the non-interfering short-long and long-short events, whereas the central peaks show interference due to the indistinguishability of the short-short and long-long contributions. The clear resolution of the satellite peaks arises from the low

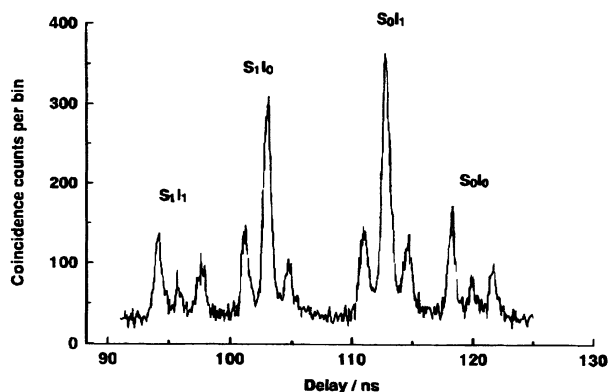


FIG. 3. A typical time delay spectrum showing twelve peaks grouped into four sets of three. Each set of three corresponds to one pair of detectors as labeled. The four central peaks display the interference. The two inner central peaks are clearly enhanced and the two outer ones suppressed. Collection bin widths were 79 ps and experiment duration about 1 min.

combined detection time jitter of 750 ps FWHM which is smaller than peak separation due to the 1.7 ns delay.

This interference effect is dramatically displayed in Fig. 3 where two of the central peaks are enhanced and two suppressed as predicted by Eq. (4). This is a clear indication that the total coincidence rate remains constant while changes in phase redistribute the coincidences between the detectors. Further adjustment of both polarization controllers is necessary to maximize this effect. The number of counts in 6 s in the four central peaks (around 1900 counts) is recorded as a function of translation stage position. The background coincidence count associated with random overlap of pulses within the coincidence peak width, typically around 1.5 ns, is estimated from the average number of counts per time bin outside the triplets and subtracted from the peak counts. The remaining counts can be assumed proportional to the probabilities  $P_{si}(p, q)$  and used to calculate the correlation coefficient  $E$  as in Eq. (5). Figure 4 shows  $E$  as a function of air gap length change fitted by a cosinusoidal function of visibility 86.9%  $\pm$  1.2%. The wavelength of the oscillation is less than 820 nm due to small temperature drifts (the interferometers are housed in separate polystyrene enclosures) leading to a slow drift of phase (about 0.5 rad/min here). Although we do not actively change the phase of the 1.3  $\mu$ m interferometer, this slow drift does ensure that a range of  $\phi_s > \pi/2$  is explored in the measurement shown. This, in principle, allows us to claim a violation of Bell's inequality based on this measurement alone [15] although a much more careful thermal control and active scanning of  $\phi_s$  is intended for a future experiment.

Deviation from the theoretical maximum visibility of 100% is due to several factors. Loss of light across the air gap (0.7 transmission) and slight deviations of the beam splitter ratios from 50/50 reduces visibility by 1% at most. Imperfect peak separation due to detector time jitter and incorrect background estimation adds 3%. The effects of second order dispersion could add another 1%, but we have not quantified the effect of third order terms. We believe the bulk of the visibility loss (7%–8%) arises in imperfect

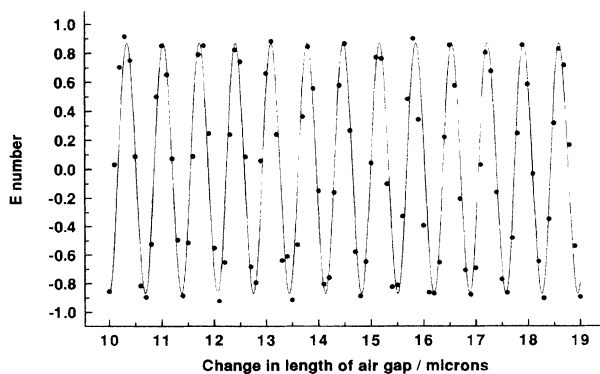


FIG. 4. Correlation coefficient  $E$  as a function of air gap length change (arbitrary origin). Experimental data points are fitted by a cosinusoidal function of visibility  $V = 86.9\% \pm 1.2\%$ .

orientation of polarization controllers. An experiment with the 4.3 km reel of fiber removed showed a small *reduction* in visibility from the above which could be regained by reoptimization of the polarization controller indicating that there may be some polarization effects in the couplers.

In conclusion, we have seen strong correlations of quantum mechanical origin at locations separated by 4.3 km of coiled optical fiber. These correlations do not appear to decrease with distance traveled in fiber. We expect that future experiments with a real space separation of some kilometers will not change this result. With further optimization of visibility such an arrangement could be used for quantum cryptography [8].

This work was funded in part by the European community via ESPRIT Grant No. BRA6934. We also acknowledge helpful discussions with Dr. M. Reck and Dr. T. Larchuk during the preparation of this work.

- [1] B. R. Mollow, Phys. Rev. A **8**, 2864 (1973).
- [2] J. S. Bell, Physics **1**, 195 (1964).
- [3] S. J. Freedman and J. F. Clauser, Phys. Rev. Lett. **28**, 938–941 (1972); J. F. Clauser, Phys. Rev. Lett. **36**, 1223 (1976); E. S. Fry and R. C. Thompson, Phys. Rev. Lett. **37**, 465 (1976); A. Aspect, J. Dalibard, and G. Roger, Phys. Rev. Lett. **49**, 1804–1807 (1982); W. Perrie, A. J. Duncan, H. J. Beyer, and H. Kleinpoppen, Phys. Rev. Lett. **54**, 1790, E2647 (1985); Z. Y. Ou and L. Mandel, Phys. Rev. Lett. **61**, 50–53 (1988); Y. H. Shih and C. O. Alley, Phys. Rev. Lett. **61**, 2921 (1988).
- [4] M. A. Horne, A. Shimony, and A. Zeilinger, Phys. Rev. Lett. **62**, 2209–2212 (1989); M. A. Horne and A. Zeilinger, in *Symposium on the Foundations of Modern Physics*, edited by P. Lahti and P. Mittelstaedt (World Scientific, Singapore, 1985), p. 435–439.
- [5] J. G. Rarity and P. R. Tapster, Phys. Rev. Lett. **64**, 2495 (1990).
- [6] J. D. Franson, Phys. Rev. Lett. **62**, 2205 (1989).
- [7] J. Brendel, E. Mohler, and W. Martienssen, Europhys. Lett. **20**, 575 (1992); P. G. Kwiat, A. M. Steinberg, and R. Y. Chiao, Phys. Rev. A **47**, R2472 (1993).
- [8] A. K. Ekert, J. G. Rarity, P. R. Tapster, and M. Palma, Phys. Rev. Lett. **69**, 1293 (1992).
- [9] C. H. Bennett, G. Brassard, C. Crepeau, R. Jozsa, A. Peres, and W. K. Wootters, Phys. Rev. Lett. **70**, 1895 (1993).
- [10] J. G. Rarity and P. R. Tapster, Phys. Rev. A **45**, 2052 (1992).
- [11] Y. H. Shih, A. V. Sergienko, and M. H. Rubin, Phys. Rev. A **47**, 1288 (1993).
- [12] J. D. Franson, Phys. Rev. A **44**, 4552 (1991).
- [13] J. Brendel, E. Mohler, and W. Martienssen, Phys. Rev. Lett. **66**, 1142 (1991).
- [14] J. G. Rarity, J. Burnett, P. R. Tapster, and R. Paschotta, Europhys. Lett. **22**, 95 (1993).
- [15] M. Zukowski, Phys. Lett. A **177**, 290 (1993).
- [16] This corrects a slight error in Eq. (7) of [14].
- [17] R. G. W. Brown, K. D. Ridley, and J. G. Rarity, Appl. Opt. **25**, 4122 (1986).
- [18] P. C. M. Owens, J. G. Rarity, P. R. Tapster, and D. Knight (to be published).